Cancer Cell
Article

MALT1 Small Molecule Inhibitors Specifically Suppress ABC-DLBCL In Vitro and In Vivo

Lorena Fontan,[1,2,5,11] Chenghua Yang,[3,11,12] Venkataraman Kabaleeswaran,[3,6,7] Laurent Volpon,[8] Michael J. Osborne,[8] Elena Beltran,[5] Monica Garcia,[1,2] Leandro Cerchietti,[1] Rita Shaknovich,[1,4] Shao Ning Yang,[1] Fang Fang,[1,2] Randy D. Gascoyne,[9] Jose Angel Martinez-Climent,[5] J. Fraser Glickman,[10] Katherine Borden,[8] Hao Wu,[3,6,7,*] and Ari Melnick[1,2,*]

[1]Division of Hematology and Medical Oncology
[2]Department of Pharmacology
[3]Department of Biochemistry
[4]Division of Immunopathology, Department of Pathology
Weill Cornell Medical College, New York, NY 10021, USA
[5]Division of Oncology, Center for Applied Medical Research, University of Navarra, 31008 Pamplona, Navarra, Spain
[6]Program in Cellular and Molecular Medicine, Children's Hospital Boston, Boston, MA 02115, USA
[7]Department of Biological Chemistry and Molecular Pharmacology, Harvard Medical School, Boston, MA 02115, USA
[8]Institute for Research in Immunology and Cancer, University of Montreal, Montreal QC H3C 3J7, Canada
[9]Centre for Lymphoid Cancer, BC Cancer Agency, Vancouver, BC V5Z 1L3, Canada
[10]High-Throughput Screening Resource Center, The Rockefeller University, New York, NY 10065, USA
[11]These authors contributed equally to this work
[12]Present address: Department of Molecular Pharmacology and Chemistry, Sloan-Kettering Institute, New York, NY 10021, USA
*Correspondence: hao.wu@childrens.harvard.edu (H.W.), amm2014@med.cornell.edu (A.M.)
http://dx.doi.org/10.1016/j.ccr.2012.11.003

SUMMARY

MALT1 cleavage activity is linked to the pathogenesis of activated B cell-like diffuse large B cell lymphoma (ABC-DLBCL), a chemoresistant form of DLBCL. We developed a MALT1 activity assay and identified chemically diverse MALT1 inhibitors. A selected lead compound, MI-2, featured direct binding to MALT1 and suppression of its protease function. MI-2 concentrated within human ABC-DLBCL cells and irreversibly inhibited cleavage of MALT1 substrates. This was accompanied by NF-κB reporter activity suppression, c-REL nuclear localization inhibition, and NF-κB target gene downregulation. Most notably, MI-2 was nontoxic to mice, and displayed selective activity against ABC-DLBCL cell lines in vitro and xenotransplanted ABC-DLBCL tumors in vivo. The compound was also effective against primary human non-germinal center B cell-like DLBCLs ex vivo.

INTRODUCTION

Non-Hodgkin's lymphoma (NHL) is the seventh most frequent cancer (Siegel et al., 2012). Diffuse large B cell lymphoma (DLBCL) is the most common subtype of NHL, accounting for ~25% of all lymphoma cases (Swerdlow et al., 2008). Gene expression profiling allowed subclassification of DLBCL into distinct molecular subtypes, including germinal center B cell-like (GCB) DLBCL, activated B cell-like (ABC) DLBCL, and primary mediastinal B cell lymphoma (PMBL) (Alizadeh et al., 2000; Rosenwald et al., 2003). These subtypes differ significantly in their spectrum of recurrent somatic mutations, dependence on different signaling pathways, and response to current standard therapies (Lenz et al., 2008b; Wright et al., 2003). Patients with the GCB subtype have a significantly better overall survival compared to those with the ABC subtype (Alizadeh et al., 2000;

Significance

MALT1 is a unique paracaspase protein that transduces aberrant oncogenic signaling in ABC-DLBCL. This manuscript reports the development of a constitutively activated form of MALT1 that enabled a screen for small molecule inhibitors. This led to identification of MI-2, an irreversible MALT1 protease inhibitor, which is a lead compound with nanomolar activity in cell-based assays and selective activity against ABC-DLBCLs. Importantly, we show that MALT1 inhibitors kill ABC-DLBCLs in vitro and in vivo, are nontoxic to animals, and also suppress primary human non-GCB-DLBCL specimens. Hence, we demonstrate that MALT1 is a bona fide therapeutic target and provide a lead compound that forms the basis of a class of therapeutic agents for B cell lymphomas.

Rosenwald et al., 2002). Improved therapies are needed for all DLBCLs but most urgently for ABC-DLBCLs, which are the most chemoresistant.

ABC-DLBCL is characterized by its reliance on the oncogenic activation of the NF-κB pathway through several different mechanisms. These mostly involve somatic mutations in molecules participating in signaling downstream of the B cell receptor (BCR), including activating mutations of *CARMA1/CARD11* (Lenz et al., 2008a) and *CD79A/B* (Davis et al., 2010), homozygous deletion/inactivating mutations of *TNFAIP3/A20* (Compagno et al., 2009; Honma et al., 2009), and activating mutations of *MYD88* downstream of the Toll-like receptor (Ngo et al., 2011). CARMA1 forms part of the CARMA1-BCL10-MALT1 (CBM) complex and mediates NF-κB activation downstream of the B cell receptor, T cell receptor (Ruefli-Brasse et al., 2003; Ruland et al., 2003), and ITAM-coupled natural killer cell receptors (Gross et al., 2008). The MALT1 (mucosa-associated lymphoid tissue lymphoma translocation 1) subunit is the active signaling component of the CBM complex (Lucas et al., 2001) and features protease activity that cleaves and inactivates inhibitors of the NF-κB signaling pathway such as TNFAIP3/A20 (Coornaert et al., 2008), CYLD (Staal et al., 2011), and RELB (Hailfinger et al., 2011) or the BCL10 protein (Rebeaud et al., 2008), indirectly activating NF-κB signaling. *MALT1* translocations, including t(11;18)(q21;q21), which produces an *API2-MALT1* fusion, and t(14;18)(q32;q21), which results in the *IGH-MALT1* translocation, are detected in up to 55% of MALT-type lymphomas (Farinha and Gascoyne, 2005). These translocations lead to overexpression of *MALT1* and, in the case of the *API2-MALT1* translocation, constitutive activation of the pathway (Dierlamm et al., 1999; Sanchez-Izquierdo et al., 2003; Streubel et al., 2003). Constitutive expression of MALT1 in mice induces a disease that is similar to MALT lymphomas in humans, and induces ABC-like DLBCLs in a p53-null background (Vicente-Dueñas et al., 2012). *MALT1* has not been found mutated or translocated in DLBCL but is gained along with *BCL2*, and this low-copy-number amplification is associated with an ABC-DLBCL phenotype (Dierlamm et al., 2008). Moreover, ABC-DLBCL cell lines have been shown to be dependent on MALT1 catalytic activity (Ferch et al., 2009; Hailfinger et al., 2009; Ngo et al., 2006).

MALT1 is a paracaspase, which is related to the caspase (cysteine-*asp*artic prote*ases*) family of proteases but cleaves after Arg residues instead of Asp (Rebeaud et al., 2008). *MALT1* is the only gene encoding paracaspase in the human genome. MALT1-null animals display defects in B and T cell function but are otherwise healthy (Ruefli-Brasse et al., 2003; Ruland et al., 2003). These factors suggest that MALT1-targeted therapy would likely be well tolerated with little or manageable toxicity. Consequently, MALT1 represents a potentially important therapeutic target for ABC-DLBCL and MALT lymphoma.

RESULTS

Biochemical Screening Identifies Low Molecular Weight Inhibitors of MALT1 Proteolytic Activity

We reasoned that MALT1 small molecule inhibitors might be useful chemical tools for studying MALT1 biology and treating MALT1-addicted tumors. However, full length MALT1 and its paracaspase domain (amino acids 340–789) are naturally present in physiological solutions as a monomer, which has very low proteolytic activity. Caspases generally must homodimerize for maximal catalytic activity (Pop et al., 2006; Walker et al., 1994; Yin et al., 2006), and accordingly the recently reported structures of the paracaspase domain of MALT1 in complex with a peptide inhibitor are dimeric (Wiesmann et al., 2012; Yu et al., 2011). In order to generate catalytically active MALT1 for an effective assay to screen for inhibitors, we biochemically engineered a recombinant form of MALT1 (340–789) fused with a leucine zipper dimerization motif (LZ-MALT1), which promotes its dimerization and activation (Figure 1A). We developed a MALT1 activity assay using the MALT1 substrate peptide LRSR linked to the fluorogen AMC (7-amino-4-methylcoumarin). Cleavage of the Ac-LRSR-AMC substrate by MALT1 resulted in release of AMC and a fluorescent signal.

The optimal conditions for high-throughput screening were determined by systematic variation of the concentrations of the enzyme and the substrate in a two-dimensional grid. Fluorescence measurements were taken every 45 s for 60 min. The measurements were plotted as a function of time. Conditions with a linear relationship between fluorescence and time were considered appropriate for screening. Quality was assessed using the Z′ factor, a coefficient reflective of the dynamic range of the assay and variance of the data (Zhang et al., 1999), calculated by the formula $Z'\ \text{factor} = 1 - 3 \times (\sigma_p + \sigma_n)/(|\mu_p - \mu_n|)$, where $\sigma_{p/n}$ is the standard deviation for positive and negative control and $\mu_{p/n}$ is the mean for positive and negative control. The Z′ factor for this screen was 0.738, which is within the optimal range 0.5–1 (Zhang et al., 1999). A total of 46,464 compounds was screened (see Supplemental Experimental Procedures available online). Using 40% inhibition as a threshold, 324 candidate compounds were selected for validation in a concentration-response assay (Figure 1B). Of these, 19 compounds (Figure S1A) were selected for further validation based on their biochemical activity (half-maximal inhibitory concentration [IC_{50}] < 20 μM; Figure 1C).

Candidate Inhibitors Selectively Suppress ABC-DLBCL Cell Lines and MALT1 Catalytic Activity

MALT1 activity plays an important role in selectively maintaining proliferation of ABC-DLBCL cell lines (Ngo et al., 2006). Accordingly, ABC- and GCB-DLBCL cell lines present differential sensitivity to MALT1 cleavage inhibition by the peptide Z-VRPR-FMK (Ferch et al., 2009; Hailfinger et al., 2009; Rebeaud et al., 2008). To determine whether candidate small molecules display a similar profile, two ABC-DLBCL cell lines, HBL-1 and TMD8, and one GCB-DLBCL cell line, OCI-Ly1, were exposed to increasing concentrations of the 19 selected molecules. Cell proliferation was measured 48 hr after exposure to a single dose of compound using an ATP-based metabolic luminescent assay (summarized in Figure 1C). Three compounds consistently induced significant selective dose-dependent suppression of ABC-DLBCL cells (MI-2, $p < 0.0001$; MI-4, $p = 0.006$; MI-11, $p < 0.0001$; regression extra sum-of-squares F test; Figures 1C and S1B). Hence, these compounds were active in cells, selective for ABC-DLBCLs, and lack nonspecific cellular toxicity. MI-6 and MI-15 also showed differential inhibition of ABC-DLBCL cells but did not reach statistical significance.

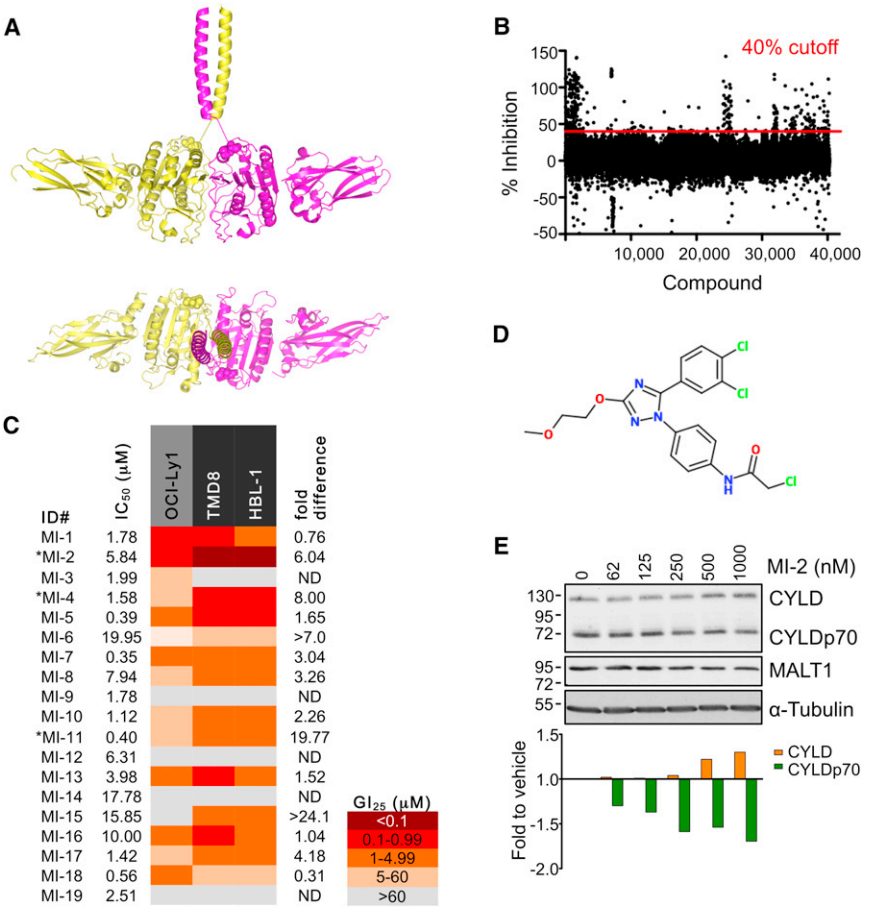

Figure 1. Identification of MALT1 Small Molecule Inhibitors

(A) Dimeric LZ-MALT1 representation showing LZ-MALT1 monomers in yellow and magenta. Met338 is shown as a sphere model. The model was generated using the MALT1 structure (Protein Data Bank [PDB] ID code 3UOA) and LZ structure (PDB ID code 2ZTA).

(B) Represented is the % inhibition for each of the compounds assayed at 12.5 μM. Cutoff was 40% inhibition.

(C) Summary table of IC_{50} and GI_{25} results for screening hits. Experiments were performed three times in triplicate. Fold difference = OCI-Ly1 GI_{25}/average GI_{25} for the MALT1-dependent cell lines. *Significant dose-dependent suppression of proliferation in ABC-DLBCL, regression extra sum-of-squares F test.

(D) MI-2 structure.

(E) MALT1 cleavage of CYLD inhibition by MI-2 in HBL-1 cells at 24 hr studied by western blot. α-tubulin, and loading control. Densitometry values were normalized to α-tubulin and are relative to vehicle-treated cells. The representative result is from three experiments.

See also Figure S1.

Compound MI-2 was the most potent in cell-based assays, with 25% growth-inhibitory concentration (GI_{25}) values in the high-nanomolar range. MI-2 (Figure 1D) was therefore next assayed for inhibition of MALT1-mediated substrate cleavage in lymphoma cells. HBL-1 cells were treated with increasing concentrations of MI-2 for 24 hr and cleavage of the MALT1 target protein CYLD was measured by western blotting and densitometry. MI-2 caused a dose-dependent decrease in MALT1-mediated cleavage, noted by an increase in the uncleaved CYLD protein and a decrease in the cleaved form of the protein (Figure 1E). MI-2 was selective as a MALT1 paracaspase inhibitor, because it displayed little activity against the structurally related caspase family members caspase-3, -8, and -9 (Figure S1C). Moreover, MI-2 did not inhibit caspase-3/7 activity or apoptosis in cell-based assays at concentrations that suppress MALT1 (Figures S1D–S1F). Hence, MI-2 is a potential lead compound as a therapeutic MALT1 inhibitor.

MI-2 Analogs Display MALT1-Inhibitory Activity

To establish whether compound MI-2 represented a potential scaffold for development of MALT1 inhibitors, we compared MI-2 with other chemical compounds in silico to identify potential analogs. A total of 704 analog compounds from available libraries with similarity score ≥70% (Tanimoto similarity functions) was screened by LZ-MALT1 fluorescence assay. Nineteen analogs displaying equal or higher activity than MI-2 were selected (Figure 2A). Five analogs with biochemical IC_{50}s within a similar range as MI-2 were selected for further characterization in cell-proliferation assays (Figures 2B and 2C). All five analogs (MI-2A1–5) exhibited the same trend toward selective suppression of the ABC-DLBCL cell lines, with GI_{25} concentrations in the micromolar range (Figure 2C). Two analog compounds with no LZ-MALT1-inhibitory activity in vitro (MI-2A6 and -7) used as chemical controls had no effect on cell proliferation over the same dose range (Figure S2). The five active MI-2 analogs were assayed for inhibition of MALT1 cleavage of CYLD. All five compounds, administered at 5 μM for 8 hr, showed cleavage inhibition similar to the Z-VRPR-FMK MALT1 blocking peptide (50 μM) used as positive control (Figure 2D), although MI-2 itself remained the most potent compound. Collectively, the conservation of MALT1 inhibitor activity in vitro and in cell-based assays among chemically related compounds points toward the suitability of MI-2 and its analogs as lead compound inhibitors of MALT1.

MI-2 Directly Binds and Irreversibly Inhibits MALT1

We next investigated whether MI-2 directly bound to MALT1 or indirectly affected MALT1 activity, for example through binding to the LZ region of the fusion protein. Heteronuclear single-quantum coherence (HSQC) nuclear magnetic resonance (NMR) spectroscopy was used to characterize the binding of MI-2 to the paracaspase domain of MALT1 (residues 329–728). As MI-2 was titrated in, resonances corresponding to the unbound state of MALT1 decreased in intensity, while another set of resonances corresponding to the MALT1-MI-2 complex gradually appeared (Figure 3A). This pattern of chemical shift changes is characteristic of slow exchange on the NMR

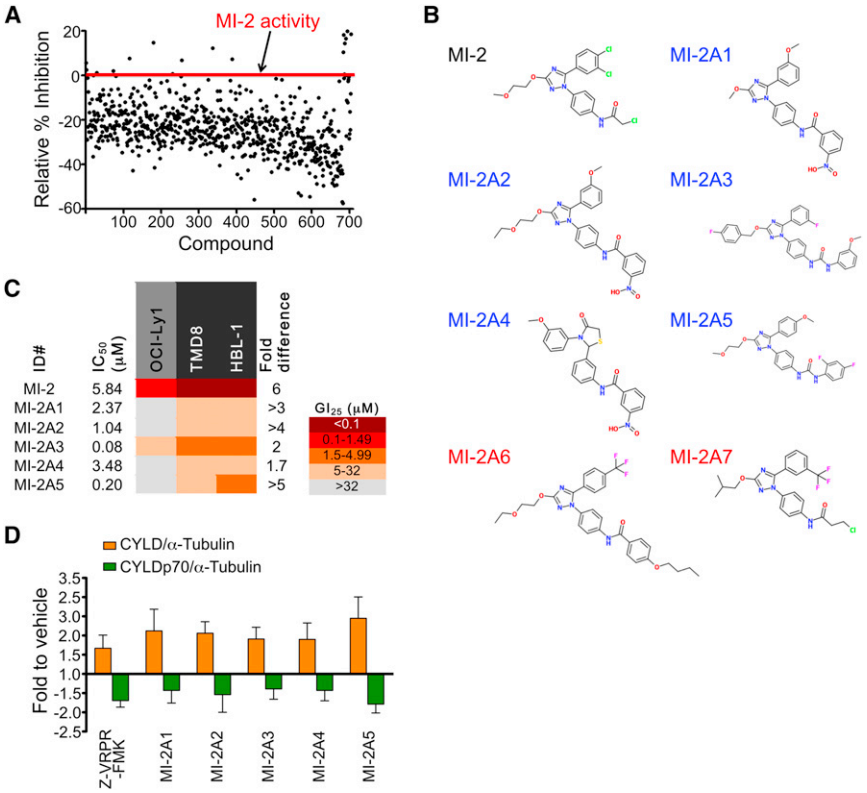

Figure 2. MI-2 Analogs Display Similar MALT1-Inhibition Activity

(A) Seven hundred and four compounds with over 70% homology to MI-2 were screened. Compounds with equal or higher activity than MI-2 were selected.

(B) Structures of the MI-2 analog compounds assayed in cell growth-inhibition experiments. Blue, active analogs; red, inactive analogs.

(C) IC_{50} and GI_{25} values for the selected analogs assayed in HBL-1, TMD8, and OCI-Ly1 cells. Experiments were performed three times in triplicate. Fold difference = OCI-Ly1 GI_{25}/average GI_{25} for the MALT1-dependent cell lines.

(D) CYLD cleavage was studied in HBL-1 cells treated with 5 μM analog compound or 50 μM Z-VRPR-FMK for 8 hr. Densitometry results were normalized to α-tubulin and fold change-to-vehicle ratios were calculated. Results are mean ± SEM of three independent experiments.

See also Figure S2.

timescale and is indicative of a robust interaction between MALT1 and MI-2. In contrast, NMR spectroscopy studies showed no evidence of binding by the inactive analogs MI-2A6 and MI-2A7 (Figure 3B).

Because MI-2 contains a reactive chloromethyl amide, we investigated whether MI-2 could modify MALT1 covalently using liquid chromatography-mass spectrometry (LC-MS). As shown in Figure 3C, MALT1 paracaspase domain (329–728) presented a major peak at 55,988.4 Da. Upon incubation with the compound MI-2, the major peak of MALT1 was shifted to 56,407.5 Da, an increase of 419.1 Da. This corresponds to addition of MI-2 minus the chloride group, indicating that MI-2 can bind covalently to MALT1 and potentially act as an irreversible inhibitor. Because the chloromethyl amide group is not conserved in the active MI-2 analogs (Figure 2B), it is most likely the common chemical scaffold in the MI-2 series that provides specificity to MALT1. Notably, LC-MS performed with MI-2 and the MALT1 active site mutant C464A revealed markedly reduced covalent binding, suggesting that the active site C464 residue is the main target of modification by MI-2 (Figure 3C). To further explore the potential mode of binding of MI-2 to the MALT1 paracaspase domain, we employed molecular docking using AutoDock 4.2 (Morris et al., 2009). The crystal structure of MALT1 (Wiesmann et al., 2012; Yu et al., 2011) was kept as a rigid body while allowing conformational flexibility of MI-2. The final results were ranked on the predicted binding free energy and the cluster size for each docking conformation. The top five poses were selected, all of which had similar docking scores with slight changes in their orientations. As shown for the first top hit, MI-2 appears to bind the active site cleft with its chloromethyl group close to the active site C464 in the paracaspase domain (Figures 3D and S3A), consistent with a covalent-bond formation between these two groups. Collectively, the data suggest that MI-2 engages and irreversibly binds the MALT1 active site.

To examine whether MI-2 inhibition of MALT1 is consistent with irreversible binding kinetics, LZ-MALT1 was preincubated with different concentrations of MI-2 for 5–80 min followed by addition of the substrate Ac-LRSR-AMC to determine enzymatic activity (Figures 3E and S3B). Notably, the percent MALT1 inactivation increased with time, reaching plateaus near the end of the test, consistent with covalent and irreversible inhibition. Inhibition was concentration dependent, with higher concentrations showing greater inactivation and faster rates of saturation. In contrast, the active MI-2 analog MI-2A2, which does not have the chloromethyl amide group, showed no evidence of cumulative inhibition of MALT1, consistent with reversible inhibition. It should be noted that MI-2 reached close to 100% inhibition, whereas MI-2A2 with a lower IC_{50} only reached ~50% inhibition (Figure 3E). The irreversible kinetics might contribute to the more potent effects of MI-2 in cell-based assays versus its analogs that lack the chloromethyl amide group and only bind reversibly, as has been noted in the case of peptidyl halomethyl ketone protease inhibitors (Powers et al., 2002).

MI-2 Inhibits MALT1 Functions in ABC-DLBCL Cell Lines

Having confirmed MI-2 as a lead compound, we next explored its effects on MALT1 signaling in ABC-DLBCL cells. We first examined the impact of MI-2 on cleavage of additional MALT1 substrates such as A20, BCL10, and RELB. Because these proteins are directed to proteasomal degradation after cleavage (Coornaert et al., 2008; Hailfinger et al., 2011; Rebeaud et al., 2008), we used the proteasome inhibitor MG-132 to facilitate visualization of cleavage products (Figure 4A). HBL-1 and

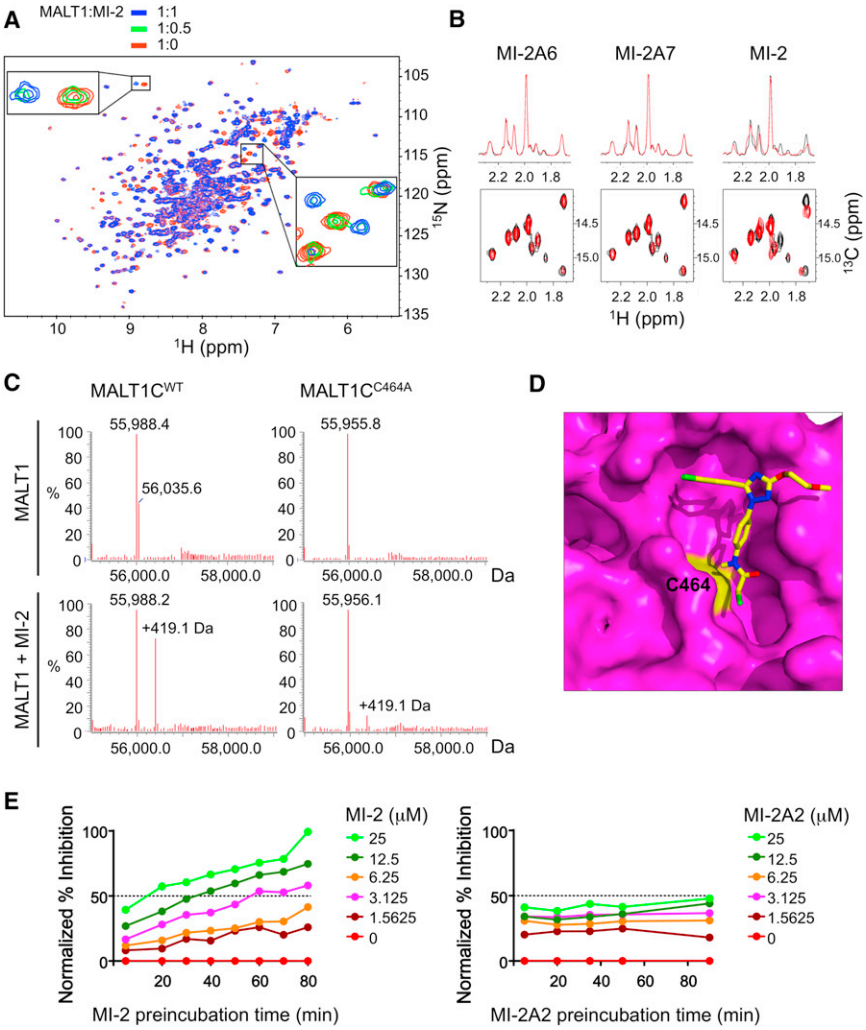

Figure 3. MI-2 Directly Interacts with and Irreversibly Inhibits MALT1

(A) Superposition of the ^{1}H-^{15}N HSQC spectrum of the apo-MALT1 (red) with the MALT1-MI-2 complex (blue) at a molar ratio of 1:1. The expanded regions highlight interacting residues in the slow-exchange regime on the NMR timescale (intermediate 1:0.5 MALT1:MI-2 ratio is shown in green).

(B) One-dimensional (top) and two-dimensional (bottom) ^{1}H-^{13}C HSQC NMR spectra of MALT1 (329–728) without (black) and with compounds MI-2A6, MI-2A7, and MI-2 (red).

(C) LC-MS for MALT1^{WT} and MALT1^{C464A} (amino acids 329–728) with and without MI-2.

(D) Docked MI-2 (in stick model) on the MALT1 paracaspase domain (in surface representation). MALT1 is shown in magenta with C464 in yellow. MI-2 is shown with carbons in yellow, oxygens in red, nitrogens in blue, and chlorines in green.

(E) LZ-MALT1 was preincubated with the indicated concentrations of MI-2 or MI-2A2 (0–25 μM) for different durations (5–90 min) before Ac-LRSR-AMC was added. The graphs represent normalized % inhibition compared to preincubation time. See also Figure S3.

TMD8 cell lines were exposed to either MI-2 (2 μM) or vehicle for 30 min followed by 5 μM MG-132 for an additional 1 (lanes 2 and 3) or 2 hr (lanes 4 and 5) in order to allow cleaved forms of MALT1 substrates to accumulate during exposure to MI-2. As expected, MG-132 exposure revealed the accumulation of A20, BCL10, and RELB cleavage products due to the constitutive activity of MALT1 in these DLBCL cells. However, exposure to MI-2 diminished the abundance of cleaved forms and/or increased the abundance of full-length proteins, consistent with the loss of MALT1 enzymatic activity (Figure 4A).

MALT1 mediates c-REL translocation to the nucleus following BCR stimulation (Ferch et al., 2007). Therefore, HBL-1 cells were exposed to 200 nM MI-2, 50 μM Z-VRPR-FMK (positive control), or vehicle for 24 hr, followed by c-REL flow cytometry of whole cells or isolated nuclei. Both MI-2 and Z-VRPR-FMK reduced nuclear c-REL to a similar extent, without affecting whole-cell levels of this protein (Figure 4B). To further confirm this result, we also performed western blots for c-REL and p65 in nuclear extracts of HBL-1 and TMD8 cells treated for 24 hr with GI_{50} concentrations of MI-2 (200 nM for HBL-1 and 500 nM for TMD8). In both cell lines, exposure to MI-2 caused a clear reduction of nuclear c-REL whereas it did not affect p65 levels (Figure 4C). This selectivity toward c-REL had also been previously shown in MALT1 knockout mice and after MALT1 cleavage inhibition by the MALT1 blocking peptide Z-VRPR-FMK (Ferch et al., 2007, 2009; Hailfinger et al., 2011).

Antigen receptor-mediated NF-κB signaling partly depends on MALT1 activity (Ruefli-Brasse et al., 2003; Ruland et al., 2003). Hence, we tested the effect of MI-2 on attenuating NF-κB activation induced by phorbol 12-myristate 13-acetate (PMA)/ionomycin, which mimics BCR activation and activates MALT1-dependent cleavage (Coornaert et al., 2008; Rebeaud et al., 2008). First, 293T cells were transfected with the NF-κB reporter vector $(NF\text{-}\kappa B)_5$-luc2CP-pGL4 (harboring five copies of the NF-κB consensus-response element and a destabilized firefly luciferase) and TK-pRL control together with plasmids expressing BCL10 and either MALT1^{WT} or MALT1^{C464A} (inactive mutant). Exposure to PMA/ionomycin significantly increased luciferase activity in 293T cells when MALT1^{WT} was transfected, but not with the mutant MALT1^{C464A}. Pretreatment with MI-2 significantly inhibited NF-κB induction by PMA/ionomycin stimulation similarly to Z-VRPR-FMK, whereas it did not significantly affect that of MALT1^{C464A} (Figure 4D). HBL-1 cells are reported to exhibit chronic active B cell receptor signaling with consequent NF-κB activation (Davis et al., 2010). HBL-1 was transfected with the reporter construct $(NF\text{-}\kappa B)_5$-luc2CP-pGL4 and TK-pRL control. Treatment with MI-2 promoted a 20% and 50% reduction in NF-κB reporter activity at 8 and 24 hr, respectively. A similar result was observed for Z-VRPR-FMK (50 μM) (Figure 4E). This reduction in NF-κB reporter activity was significant at 24 hr for MI-2 and the blocking peptide Z-VRPR-FMK.

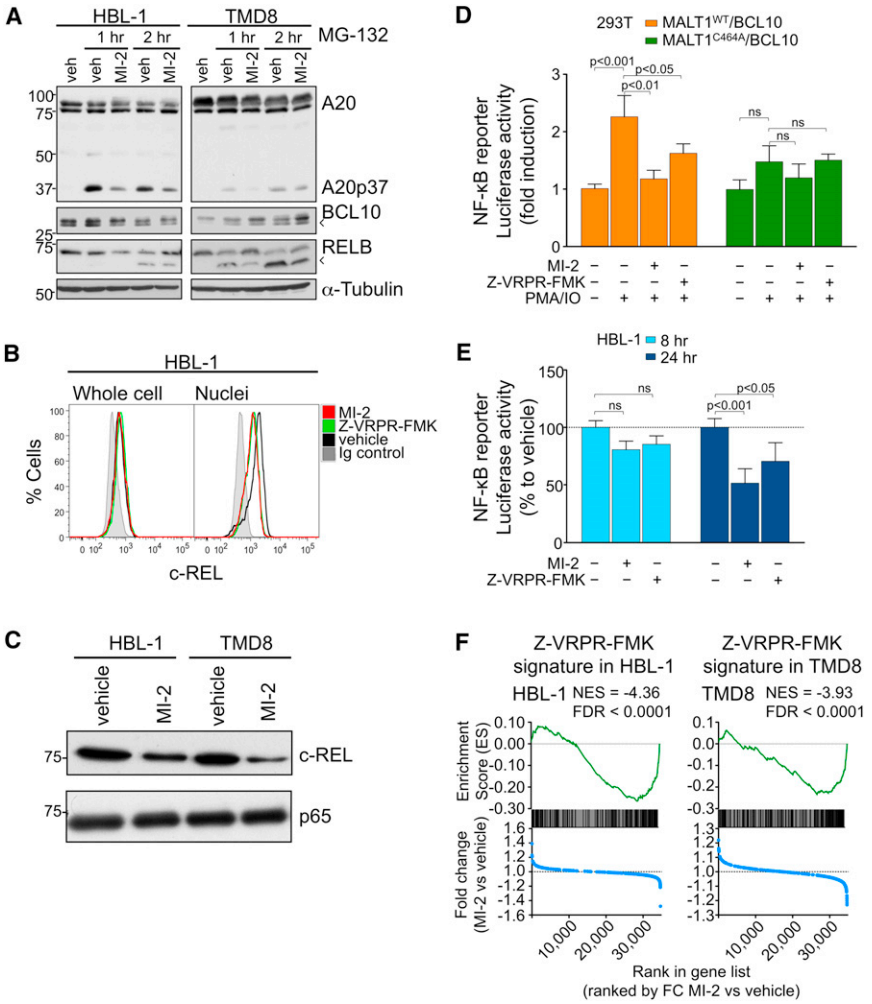

Figure 4. MI-2 Inhibits MALT1 Signaling in DLBCL Cells

(A) Western blots for A20, RELB, and BCL10 after 30 min pretreatment with 2 μM MI-2 or vehicle, followed by proteasome inhibitor MG-132 (5 μM) treatment for 1 or 2 hr in HBL-1 and TMD8. Arrowheads indicate cleavage products.

(B) Flow cytometry for c-REL whole cells or isolated nuclei from HBL-1 cells treated with 200 nM MI-2, 50 μM Z-VRPR-FMK, or vehicle for 24 hr.

(C) c-REL and p65 protein expression in nuclear extracts of HBL-1 and TMD8 cells treated for 24 hr with 200 or 500 nM MI-2, respectively.

(D) NF-κB reporter assays in 293T cells transfected with the indicated expression constructs. Cells were treated for 30 min with 2 μM MI-2, 50 μM Z-VRPR-FMK, or vehicle followed by PMA/ionomycin for 2 hr. The y axis represents luciferase fold induction relative to vehicle-treated cells, normalized to internal control. Statistics, ANOVA, Bonferroni posttest.

(E) NF-κB reporter assays in HBL-1 cells treated with 200 nM MI-2, 50 μM Z-VRPR-FMK, or vehicle for 8 and 24 hr. The y axis represents % luciferase activity relative to vehicle-treated cells, normalized to internal control. Statistics, ANOVA, Bonferroni posttest.

(F) Enrichment of Z-VRPR-FMK-downregulated genes after MI-2 treatment in HBL-1 and TMD8 cells using GSEA. Normalized enrichment score (NES) and false discovery rate (FDR) values are indicated. Top: enrichment score versus relative position of ranked genes (green tracing); bottom: fold change (FC) MI-2/vehicle versus relative position of ranked genes (blue tracing). Experiments were performed in triplicate unless otherwise specified. Data are mean ± SEM.

See also Figure S4.

The impact of MI-2 on NF-κB signaling was further characterized by gene expression profiling. For these experiments, the HBL-1 and TMD8 cell lines were treated with GI_{50} concentrations of MI-2 (HBL-1, 200 nM; TMD8, 500 nM) or 50 μM Z-VRPR-FMK for 8 hr, and RNA was extracted for gene expression studies using oligonucleotide microarrays. Z-VRPR-FMK was previously shown to attenuate the NF-κB signature in ABC-DLBCL cell lines (Hailfinger et al., 2009). MI-2 would be expected to exhibit a similar profile. For this study, we assigned Z-VRPR-FMK signatures by capturing the top 200 downregulated genes by Z-VRPR-FMK treatment compared to vehicle for each cell line. We next performed gene set enrichment analysis (GSEA) of this Z-VRPR-FMK signature against the differential expression of all genes preranked by fold change between MI-2- and vehicle-treated cells for each cell line. The Z-VRPR-FMK signature was significantly enriched among genes downregulated after MI-2 treatment for both cell lines (Figure 4F). GSEA was next performed using two independent ABC-DLBCL NF-κB gene expression signatures derived from either OCI-Ly3 and OCI-Ly10 or HBL-1 cell lines. We observed significant enrichment of these NF-κB gene sets among genes downregulated after MI-2 treatment in both cell lines (Figure S4). Collectively, these data suggest that MI-2 suppresses NF-κB activity induced by MALT1, similar to the effect observed with Z-VRPR-FMK.

MI-2 Selectively Suppresses MALT1-Dependent DLBCL Cell Lines

To further explore the spectrum of MI-2-mediated MALT1-inhibition effects, we turned to a larger panel of six ABC-DLBCL and two GCB-DLBCL cell lines (Table S1). Endogenous MALT1 activity was evaluated by western blotting for A20, BCL10, and CYLD, and NF-κB activation by phospho-IκB-α and total IκB-α (Figure S5A). Dependence on MALT1 proteolytic activity for proliferation was tested by 50 μM Z-VRPR-FMK treatment for 48 hr (Figure S5B). As expected, the two GCB-DLBCL cell lines (OCI-Ly7 and OCI-Ly1) did not display evidence of MALT1 or NF-κB signaling and did not respond to Z-VRPR-FMK. The U2932 and HLY1 ABC-DLBCL cell lines harbor mutations in TAK1 and A20, which activate NF-κB signaling downstream of MALT1. Hence, these two cell lines displayed relatively little response to Z-VRPR-FMK. In contrast, the ABC-DLBCL cells HBL-1, TMD8, OCI-Ly3, and OCI-Ly10 displayed evidence of MALT1 activity and inhibition of proliferation by Z-VRPR-FMK, indicating that these four cell lines are MALT1 dependent.

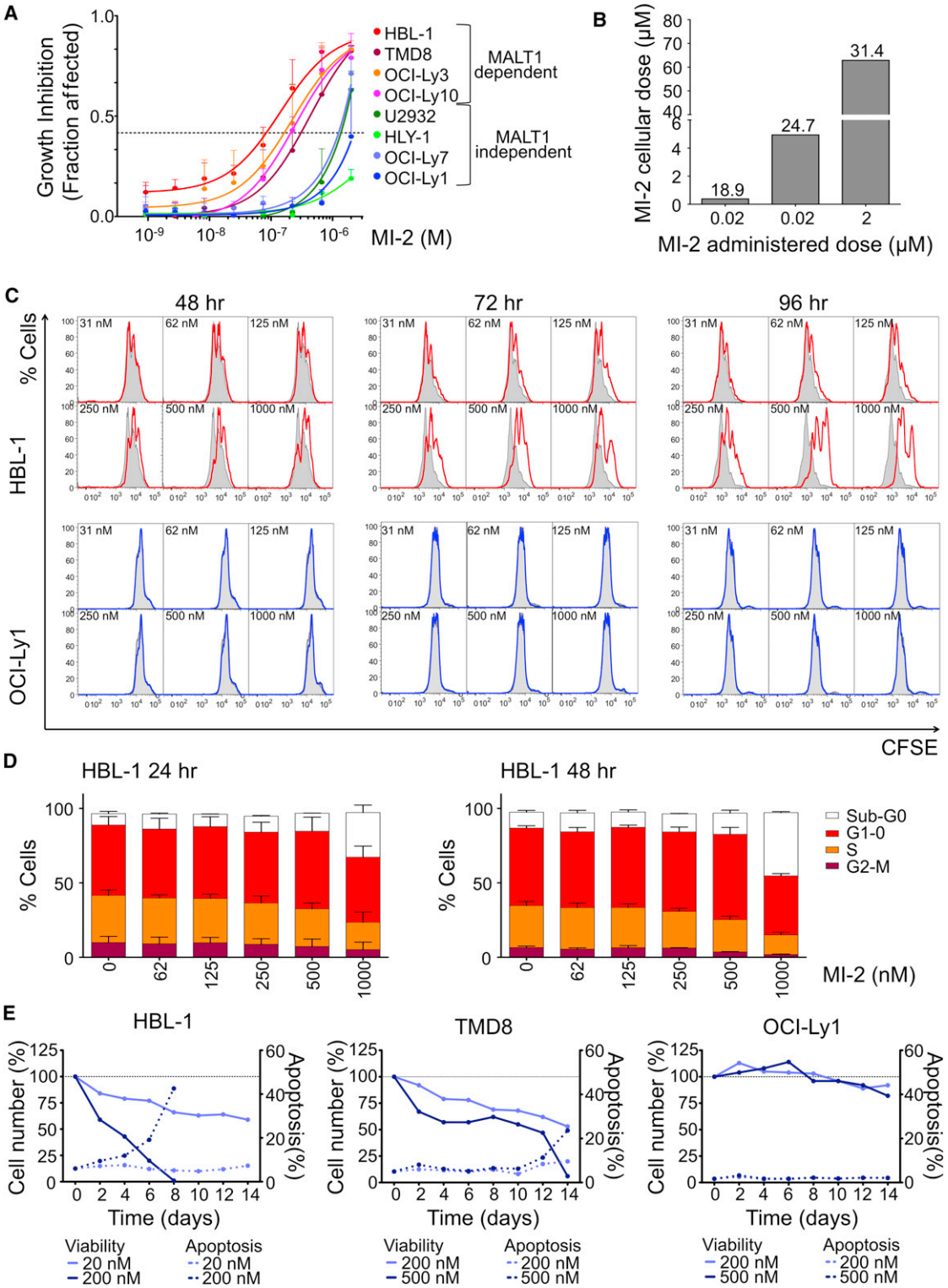

Figure 5. MI-2 Inhibits Cell Proliferation of MALT1-Dependent DLBCL Cells

(A) Dose-effect graphical representation for eight DLBCL cell lines exposed to MI-2 for 48 hr. Data are mean ± SEM of three independent experiments performed in triplicate.

(B) Intracellular MI-2 concentration determined by LC-MS in HBL-1 cells treated for 2 hr. The y axis represents MI-2 intracellular concentration. The x axis represents administered dose of MI-2. Fold-change accumulation in cells is indicated.

(C) CFSE dilution assay in HBL-1 and OCI-Ly1 cells after treatment with MI-2 for 48, 72, and 96 hr. Cells (2×10^4) were measured; $DAPI^-$ cells were gated for analysis.

All eight cell lines were exposed to increasing concentrations of MI-2 (single dose) and cell proliferation was measured at 48 hr using an ATP-based metabolic luminescent assay (Figure 5A). Growth inhibition by MI-2 was selective for MALT1-dependent cell lines, whereas the ABC-DLBCL MALT1-independent cell lines, U2932 and HLY-1, and the two GCB-DLBCL cell lines were resistant. The GI_{50} for MI-2 in HBL-1, TMD8, OCI-Ly3, and OCI-Ly10 cells was 0.2, 0.5, 0.4, and 0.4 μM, respectively, which is lower than its IC_{50} in vitro (Figure 1). This is likely explained by the irreversible binding of MI-2 to MALT1 as shown in Figure 3, but could also be due to intracellular accumulation of the compound. Indeed, we observed an 18- to 30-fold increase in MI-2 intracellular concentration in experiments where HBL-1 cells were exposed to 0.02, 0.2, or 2 μM MI-2 for 2 hr and washed three times and MI-2 was measured by LC-MS (Figure 5B). The intracellular concentration in the 0.2 μM MI-2-treated cells was 5 μM, similar to the calculated in vitro IC_{50} (Figure 5B). To determine the kinetics of accumulation of free drug, we measured the intracellular concentration of MI-2 at the GI_{50} concentration of 0.2 μM at 30 min and 2, 6, 12, 24, and 48 hr (Figure S5C). By 12 hr, there was virtually no detectable free MI-2 within the cells. However, after exposure of HBL-1 cells to increasing concentrations of a single dose of MI-2, recovery of cells only started to become evident after 48 hr (of the 0.2 μM dose level; Figure S5D). These data suggest that the potent biological effects of MI-2 are due at least in part to its irreversible binding to MALT1 aided by its tendency to concentrate in cells.

To explore in more detail the biological effects of MALT1 inhibition, HBL-1, TMD8, OCI-Ly10, and the GCB-DLBCL cell line OCI-Ly1 were treated with increasing concentrations of MI-2. Cell proliferation was examined using the 5-(and 6)-carboxyfluorescein diacetate succinimidyl ester (CFSE) dilution assay by flow cytometry on viable cells at 48, 72, and 96 hr. MI-2 substantially inhibited proliferation in HBL-1, TMD8, and OCI-Ly10 whereas it did not affect OCI-Ly1 (Figures 5C and S5E). Using BrdU incorporation-DAPI (4′,6-diamidino-2-phenylindole) staining and flow cytometry to assess the cell cycle, it was evident that MI-2 induced a dose-dependent decrease in S phase, with a reciprocal increment in the proportion of cells in G1-0 and sub-G0 (Figure 5D). To determine whether MALT1 inhibitors induced apoptosis, the ABC-DLBCL cell lines HBL-1 and TMD8 were treated daily with MI-2 at their respective GI_{25} and GI_{50}, and the control OCI-Ly1 cell line at the higher doses was used for TMD8. Trypan blue exclusion and apoptosis assessed by Annexin V^+ $DAPI^-$ flow cytometry was measured every 48 hr for a period of 14 days. Whereas MI-2 had no effect on OCI-Ly1 cells, it profoundly suppressed both HBL-1 and TMD8 cells, with the former exhibiting earlier and higher abundance of apoptotic cells (Figure 5E). Using the more sensitive caspase-3/7 cleavage assay, we observed evidence of dose-dependent apoptosis within 48 hr in both ABC-DLBCL cell lines (Figure S5F). Hence, MI-2 powerfully suppresses the growth and survival of ABC-DLBCL cell lines.

Compound MI-2 Is Nontoxic to Animals

To determine its suitability as a MALT1 lead compound for in vivo studies, we examined whether MI-2 induced toxic effects in mice. Five C57BL/6 mice were exposed to daily intraperitoneal (IP) administration of increasing doses of MI-2 ranging from 0.05 to 25 mg/kg over the course of 10 days to a cumulative dose of 51.1 mg/kg, and another five mice were exposed to vehicle only (5% DMSO, n = 5) (Figure 6A, toxicity 1). There was no evidence of lethargy, weight loss (Figure 6B, toxicity 1), or other physical indicators of sickness. To ascertain whether the maximal administered dose of 25 mg/kg is safe in a 14 day schedule, we exposed ten mice to daily IP administration of 25 mg/kg of MI-2 over 14 days to a cumulative dose of 350 mg/kg, using as controls five mice injected with vehicle only (Figure 6A, toxicity 2). Five mice were sacrificed after the 14 day course of MI-2 administration (together with the five controls) and the other five mice were sacrificed after a 10 day washout period to assess delayed toxicity. No toxic effects or other indicators of sickness, including weight loss (Figure 6B, toxicity 2) or tissue damage (macroscopic or microscopic), were noted (Figure 6C). Brain, heart, lung, liver, kidney, bowel, spleen, thymus, and bone marrow tissues were examined. Bone marrow was normocellular with trilineage maturing hematopoiesis. Myeloid-to-erythroid ratio was 4–5:1. Megakaryocytes were normal in number and distribution. There was no fibrosis or increased number of blasts or lymphocytes. Complete peripheral blood counts, biochemistry, and liver function tests were normal (Table S2), These studies established the safety of MI-2 for use in antilymphoma efficacy studies.

MI-2 Suppresses Human ABC-DLBCL Xenografts and Primary Human DLBCLs Ex Vivo

In order to determine whether MI-2 could suppress DLBCLs in vivo, we engrafted HBL-1 and TMD8 (MALT1-dependent) and OCI-Ly1 (MALT1-independent) DLBCL cells into the right flank region of nonobese diabetic/severe combined immunodeficiency (NOD-SCID) mice. Once tumors reached an average of 120 mm^3 in volume, mice were randomized to receive IP injection of MI-2 25 mg/kg/day or vehicle (5% DMSO). Animals were sacrificed 24 hr after the 14th injection. Remarkably, MI-2 profoundly suppressed the growth of both the TMD8 and HBL-1 ABC-DLBCL xenografts versus vehicle, whereas it had no effect on the growth of OCI-Ly1 tumors (Figure 7A). The fact that OCI-Ly1 tumors were unaffected suggests that MI-2 activity is due to its effects on lymphoma cells rather than the host microenvironment. Histological examination using the TUNEL assay to detect apoptotic cells showed a significant increase in apoptotic cells in MI-2-treated HBL-1 and TMD8 xenografts relative to vehicle but not in OCI-Ly1 xenografts (Figures 7B and S6A). We also observed a significant decrease in proliferation as measured by Ki-67 staining in HBL-1 and TMD8 xenografts compared to vehicle, but observed no difference in OCI-Ly1 xenografts (Figures 7C and S6B). To evaluate the effect

(D) BrdU pulse-labeled HBL-1 cells treated for 24 and 48 hr with MI-2 were analyzed by flow cytometry. The graph shows the % of cells for each cell-cycle phase for vehicle and each of the concentrations assayed. Data are mean ± SD of two independent experiments.
(E) Apoptosis time course in cell lines treated with MI-2 every 24 hr. Cells were counted using trypan blue and apoptosis was assessed by Annexin V^+ $DAPI^-$ every 48 hr for a period of 14 days. Left y axis, % cell number relative to vehicle for each time point. Right y axis, % apoptotic cells for each time point.
See also Table S1 and Figure S5.

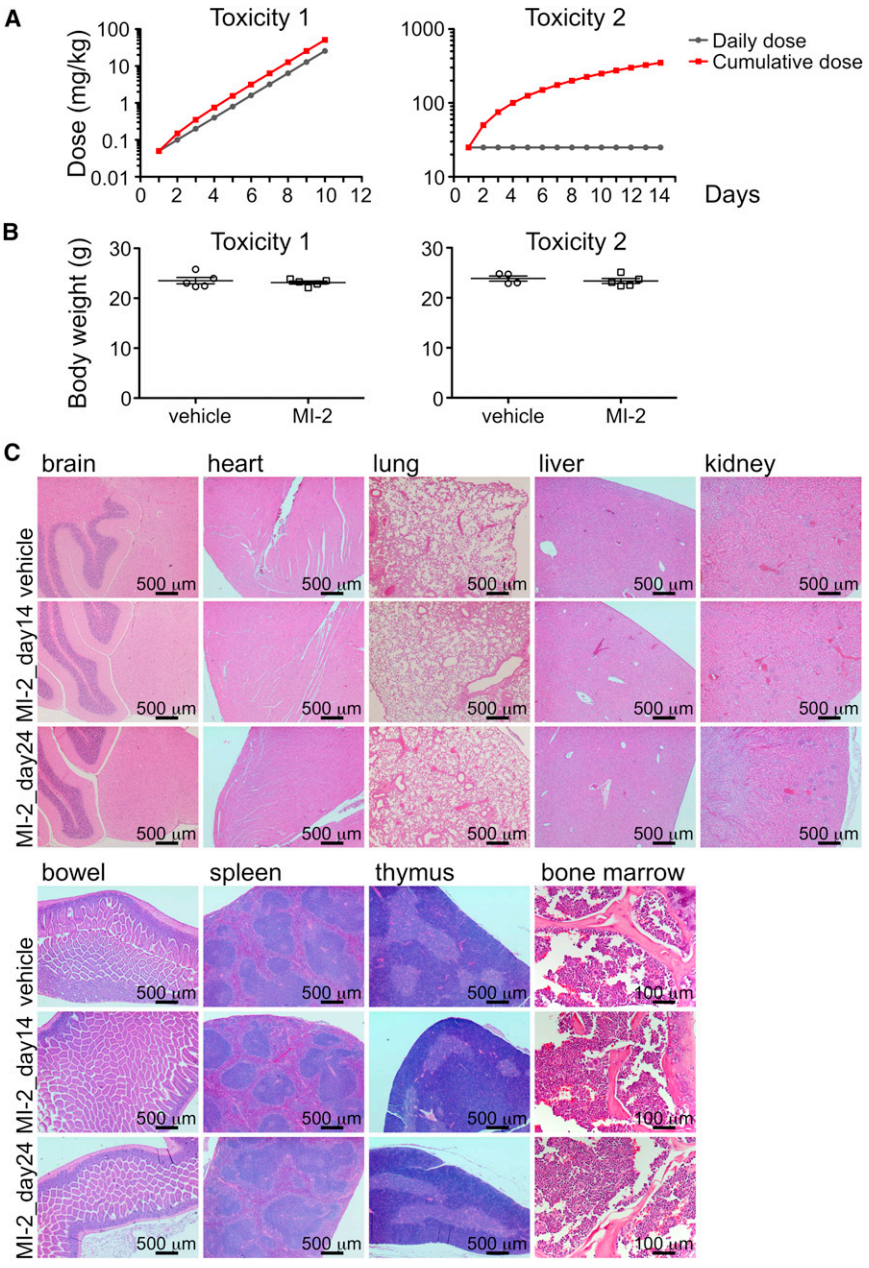

Figure 6. MI-2 Is Nontoxic to Animals

(A) Dose scheme for toxicity 1 (increasing daily dose) and toxicity 2 (same daily dose) experiments show daily and cumulative doses for each experiment.

(B) The y axis depicts mean ± SEM body weight of animals studied in both the incremental and cumulative dose schemes. Toxicity 1, $p = 0.59$ t test; toxicity 2, $p = 0.52$ t test.

(C) H&E staining for the indicated tissues in animals treated with vehicle, MI-2 25 mg/kg daily for 14 days, or MI-2 25 mg/kg daily for 14 days followed by a 10 day washout.

See also Table S2.

of MI-2 treatment on NF-κB signaling in xenografts, c-REL immunofluorescence was performed in paraffinized tumor sections. Consistent with data shown in Figures 4B and 4C, MI-2-treated tumors exhibited reduced c-REL nuclear protein (Figures 7D and S6C). Therefore, the MI-2 small-molecule MALT1 inhibitor specifically suppresses proliferation, survival, and NF-κB activity in ABC-DLBCLs in vivo in a lymphoma cell-autonomous manner.

Finally, to determine whether MI-2 could also suppress primary human DLBCLs, we obtained single-cell suspensions from lymph node biopsies of five DLBCL patients for whom their GCB versus non-GCB status could be ascertained by immunohistochemistry using the Hans criteria (Hans et al., 2004), as a surrogate for GCB versus ABC classification. Lymphoma cells were isolated and exposed to 0.8 μM MI-2 or vehicle in four replicates. After 48 hr exposure, cell number and viability were determined using trypan blue. Notably, two of the non-GCB cases responded to MI-2 ($p = 0.04$ and 0.003 versus vehicle), whereas none of the GCBs did (Figure 7E). One of the non-GCB cases did not respond to MI-2; perhaps this case was not accurately classified by Hans's criteria. Overall, these studies indicate that therapeutic targeting of MALT1 using the MI-2 small-molecule inhibitor has powerful suppressive effects on human ABC-DLBCL cells and warrants translation for use in clinical trials.

DISCUSSION

CBM complex signaling is constitutively active in a subset of ABC-DLBCLs due to somatic mutations of various genes leading to constitutive MALT1 signaling and NF-κB activation (Davis et al., 2010). The catalytic activity of MALT1 is well defined and involves substrate features such as peptide length and amino acid composition and position (Hachmann et al., 2012). Purified MALT1 is not very active in solution, because it is present as a monomer instead of its active dimeric form. Dimerization can be induced by high-salt concentrations, 1 M sodium citrate (Boatright et al., 2003). However, these high-salt conditions are nonphysiological and unsuitable for screening physiologically relevant small-molecule inhibitors. Use of a constitutively dimeric form of MALT1 enabled us to screen and identify potential inhibitors. Among these, MI-2 was found to be a potent, selective, and irreversible MALT1 inhibitor, analogous to protease inhibitor drugs such as telaprevir against the NS3/4A protease of hepatitis C virus (Klibanov et al., 2011), the proteasome inhibitor carfilzomib (Genin et al., 2010), and others (Powers et al., 2002). Although the peptide inhibitor Z-VRPR-FMK has been useful as a research tool, it is not suitable as a MALT1 therapeutic agent given its relatively large size, charge,

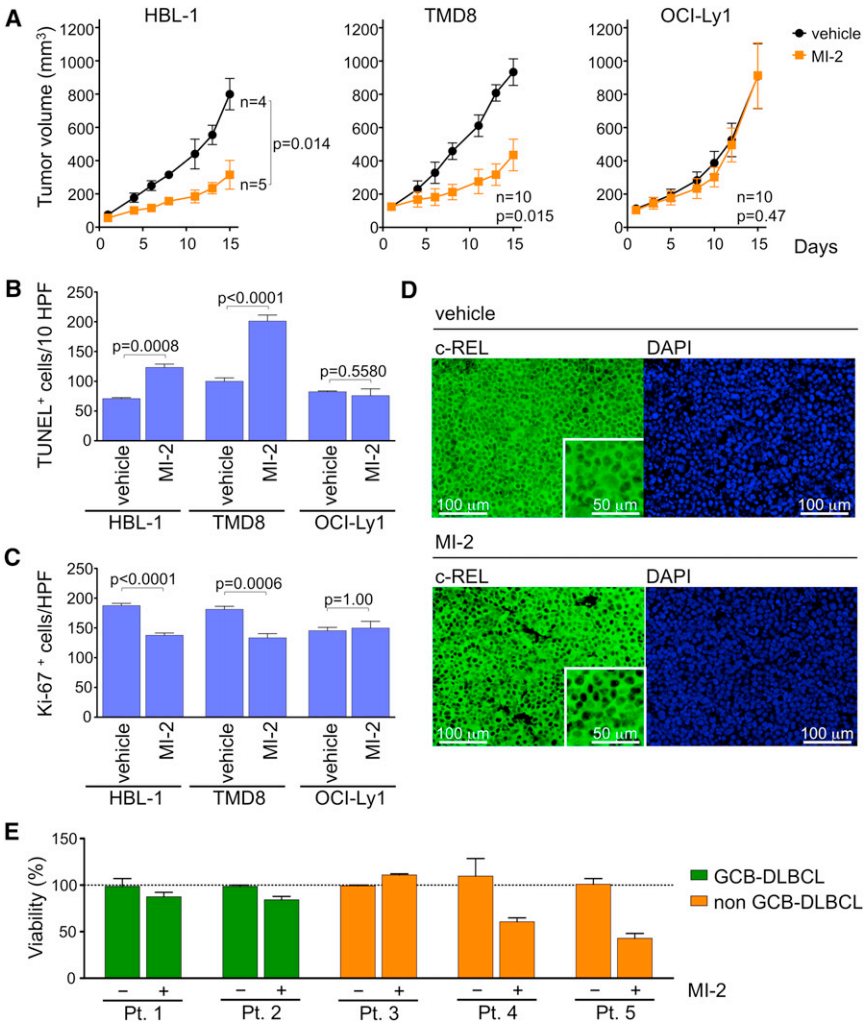

Figure 7. MI-2 Suppresses ABC-DLBCLs In Vivo and Primary Human DLBCL Ex Vivo

(A) Tumor growth curve for HBL-1, TMD8, and OCI-Ly1 xenografts in NOD-SCID mice treated with 25 mg/kg/day MI-2 or the same volume of vehicle for 14 consecutive days. Statistics, paired t test.

(B) TUNEL$^+$ staining in histologic sections of HBL-1, TMD8, and OCI-Ly1 xenografts. The y axis represents the number of TUNEL$^+$ cells per ten high-power fields (HPFs; n = 5 tumors/treatment, n = 3 for HBL-1). Statistics, t test.

(C) Ki-67 immunohistochemistry staining of xenografted HBL-1, TMD8, and OCI-Ly1 tumor sections. The y axis represents Ki-67$^+$ cells per high-power field (5 HPFs/tumor for n = 5 where analyzed for each treatment, n = 3 for HBL-1). Statistics, t test.

(D) Immunohistochemical detection of c-REL in sections from HBL-1 xenografts exposed to MI-2 or vehicle. Insets are 2× digital amplification. Representative image of three HPFs analyzed for n = 3 tumors stained for each treatment.

(E) Viability assays were performed in quadruplicate in primary human DLBCL patient samples treated for 48 hr with 0.8 μM MI-2 or vehicle. The y axis represents % of viable cells normalized to vehicle. Data are presented as mean ± SEM for all panels.

See also Figure S6.

and consequent lower cell permeability. Accordingly, MI-2 displayed superior activity in cell-based assays with excellent cell penetration and indeed featured high concentration within cells, and yet was still highly selective for MALT1 versus other caspases. Notably, a selective and irreversible small-molecule inhibitor of the tyrosine kinase BTK, PCI-32765 (ibrutinib), is currently under clinical development in patients with B cell non-Hodgkin's lymphoma (Honigberg et al., 2010). Irreversibility of MI-2 may provide pharmacokinetic advantages. As ABC-DLBCLs have chronically active BCR signaling, prolonged suppression of MALT1 cleavage would likely be necessary for maximal antilymphoma activity. Using an irreversible inhibitor, activity will only return when new enzyme is synthesized. This may allow drugs to be effective at a lower plasma concentration, thus reducing dosing level and frequency, limiting the requirement for a long plasma half-life without compromising efficacy, and minimizing potential toxic effects related to prolonged exposure to circulating drugs. Indeed, our detailed studies indicated that MI-2 was nontoxic in animals. This result is consistent with the fact that MALT1 is the only paracaspase in humans and that MALT1-deficient mice are relatively healthy (Ruefli-Brasse et al., 2003; Ruland et al., 2003).

Chronic activation of the BCR pathway in ABC-DLBCL is mediated by several different mechanisms, many of them upstream of MALT1. ABC-DLBCL is addicted to this pathway and is often specifically addicted to MALT1 cleavage activity (Ferch et al., 2009; Hailfinger et al., 2009; Ngo et al., 2006). Notably, MI-2 selectively killed ABC-DLBCL cell lines with CD79A/B, CARMA1, and/or MYD88 mutations but not those occurring in proteins downstream of MALT1, including those with A20 homozygous deletion or TAK1 mutation. These findings underline the importance of targeted resequencing of recurrently mutated alleles in lymphoma for the rational deployment of targeted therapeutics. Although the full spectrum of lymphomas that can be targeted with MALT1 inhibitors is not fully clear yet, using an ex vivo system we were able to show that primary human non-GCB-DLBCL specimens are also addicted to MALT1 and are suppressed by MI-2.

As single agents are generally not curative and rapidly generate resistance (Misale et al., 2012), there is a growing interest in combinatorial-targeted therapy. Rational combination of MALT1 cleavage inhibition could include a combination with tyrosine kinase inhibitors targeting the Src family (dasatinib, saracatinib, bosutinib, and KX01), SYK (fostamatinib disodium), or BTK (PCI-32765). These drugs would likely synergize with MALT1 cleavage inhibition of NF-κB by further inhibiting BCR signaling, including mitogen-activated protein kinases and phosphatidylinositol 3-kinase (Lim et al., 2012). Protein kinase C (PKC) inhibition would also be a potentially beneficial

combination, as it could further inhibit the NF-κB pathway, including those activities dependent on MALT1 but independent of its proteolytic activity. The PKC inhibitor sotrastaurin, in clinical trials for prevention of transplantation rejection and treatment of psoriasis (Manicassamy, 2009; Matz et al., 2011), has been recently shown to inhibit growth of ABC-DLBCL xenografted tumors (Naylor et al., 2011), pointing to its potential use as an antilymphoma therapy for this lymphoma subtype. ABC-DLBCLs also feature BCL6 translocation, SPI-B amplification, or PRDM1 deletion or mutation (Lenz and Staudt, 2010). BCL6 inhibitors promote apoptosis and cell-cycle arrest through release of critical checkpoint genes (Cerchietti et al., 2009, 2010a; Polo et al., 2004). Combination of MI-2 and BCL6 inhibitors would thus suppress two critical pathways in ABC-DLBCLs (BCL6 and NF-κB), potentially leading to therapeutic synergy. Taken together, the results reported here identify MI-2 as a lead compound targeting MALT1 and demonstrate the significance, safety, and efficacy of MALT1 as a therapeutic target and MI-2 as a therapeutic agent for the treatment of aggressive non-Hodgkin's lymphomas that are both dependent on NF-κB signals and resistant to conventional chemotherapeutic regimens.

EXPERIMENTAL PROCEDURES

Detailed experimental procedures are presented in Supplemental Experimental Procedures.

High-Throughput Screening for MALT1 Proteolytic Activity Inhibitors

Ac-LRSR-AMC was used as substrate and reactions were measured with excitation/emission wavelengths of 360/465 nm. Two time points were measured for each reaction to eliminate false positives due to compound autofluorescence. The final percent inhibition was calculated with the formula $\{[\text{fluorescence}_{\text{test compound (T2}-\text{T1)}} - \text{fluorescence}_{\text{neg ctrl (T2}-\text{T1)}}]/[\text{fluorescence}_{\text{pos ctrl (T2}-\text{T1)}} - \text{fluorescence}_{\text{neg ctrl (T2}-\text{T1)}}]\} \times 100$, where Z-VRPR-FMK (300 nM) was used as positive control and buffer only as negative control. The positive hits were validated in concentration-response experiments within a dose range of 0.122–62.5 μM to determine IC_{50} of the compounds. Activity was validated using recombinant full-length wild-type MALT1.

Growth-Inhibition Determination

Cell proliferation was determined by ATP quantification using a luminescent method (CellTiter-Glo; Promega) and trypan blue dye exclusion. Standard curves for each cell line were calculated by plotting the cell number (determined using trypan blue) against their luminescence values, and cell number was calculated accordingly. Cell viability in drug-treated cells was normalized to their respective controls (fractional viability), and results are given as 1-fractional viability. CompuSyn software (Biosoft) was used to determine GI_{25} and GI_{50} values.

Mouse Xenograft Experiments

Eight-week-old male SCID NOD.CB17-Prkdc^{scid}/J mice were purchased from Jackson Laboratories and housed in a clean environment. Mice were subcutaneously injected with low-passage 10^7 human HBL-1, TMD8, or OCI-Ly1 cells in 50% Matrigel. Treatment was initiated when tumors reached an average size of 120 mm^3. MI-2 was reconstituted in DMSO and stored at −80°C until used and was administered by intraperitoneal injection. Tumor volume was monitored by digital calipering three times a week and calculated using the formula (smallest diameter^2 × largest diameter)/2. All procedures involving animals followed National Institutes of Health protocols and were approved by the Animal Institute Committee of the Weill Cornell Medical College of Cornell University.

Primary Cells

Patient-deidentified tissues were obtained in accordance with the guidelines and approval of the University of Navarra Institutional and Weill Cornell Medical College Review Boards. Only discarded leftover tissue after diagnosis was rendered was utilized for research, in agreement with institutional review board protocol. Patient samples were processed as previously described (Cerchietti et al., 2010b). Briefly, single-cell suspensions from lymph node biopsies were obtained by physical disruption of tissues followed by cell-density gradient separation. Cell number and viability were determined by trypan blue exclusion. Primary DLBCL cells were cultured in 96-well plates. Cells were grown in RPMI medium with 20% FBS supplemented with antibiotics for 48 hr. Cells were exposed to 0.8 μM MI-2 (1 μM for Pt.2) or control (DMSO) in quadruplicate. After 48 hr of exposure, viability was determined by using trypan blue (Sigma). All samples were normalized to their own replicate control.

ACCESSION NUMBERS

The Gene Expression Omnibus accession number for the expression microarray data reported in this paper is GSE40003.

SUPPLEMENTAL INFORMATION

Supplemental Information includes six figures, two tables, and Supplemental Experimental Procedures and can be found with this article online at http://dx.doi.org/10.1016/j.ccr.2012.11.003.

ACKNOWLEDGMENTS

We thank Paulus Erbel, Martin Renatus, and Nicola Hughes (Novartis Institutes for BioMedical Research, Basel, Switzerland) for mass spectrometry, NMR experiments, and advice; Beatriz Bellosillo (H. del Mar, Barcelona, Spain) and Miguel A. Piris (Hospital Marques de Valdecillas, Santander, Spain) for providing lymphoma samples; and Ermelinda Damko, Liwei Wang, Qi Qiao, and Jennifer Ishii for technical assistance. L.F. is supported by the Spanish Ministry of Science Fellowship "Sara Borrell." C.Y. was supported by the Irvington Institute Postdoctoral Fellowship Program of the Cancer Research Institute. H.W. and A.M. are supported by Leukemia and Lymphoma Society Translational Research Program 6210-12. A.M. is a Burroughs Wellcome Clinical Translational Scientist and is supported by the Chemotherapy Foundation and the Beverly and Raymond Sackler Center for Physical and Biomedical Sciences.

Received: August 8, 2012
Revised: October 26, 2012
Accepted: November 12, 2012
Published: December 10, 2012

REFERENCES

Alizadeh, A.A., Eisen, M.B., Davis, R.E., Ma, C., Lossos, I.S., Rosenwald, A., Boldrick, J.C., Sabet, H., Tran, T., Yu, X., et al. (2000). Distinct types of diffuse large B-cell lymphoma identified by gene expression profiling. Nature *403*, 503–511.

Boatright, K.M., Renatus, M., Scott, F.L., Sperandio, S., Shin, H., Pedersen, I.M., Ricci, J.E., Edris, W.A., Sutherlin, D.P., Green, D.R., and Salvesen, G.S. (2003). A unified model for apical caspase activation. Mol. Cell *11*, 529–541.

Cerchietti, L.C., Yang, S.N., Shaknovich, R., Hatzi, K., Polo, J.M., Chadburn, A., Dowdy, S.F., and Melnick, A. (2009). A peptomimetic inhibitor of BCL6 with potent antilymphoma effects in vitro and in vivo. Blood *113*, 3397–3405.

Cerchietti, L.C., Ghetu, A.F., Zhu, X., Da Silva, G.F., Zhong, S., Matthews, M., Bunting, K.L., Polo, J.M., Farès, C., Arrowsmith, C.H., et al. (2010a). A small-molecule inhibitor of BCL6 kills DLBCL cells in vitro and in vivo. Cancer Cell *17*, 400–411.

Cerchietti, L.C., Hatzi, K., Caldas-Lopes, E., Yang, S.N., Figueroa, M.E., Morin, R.D., Hirst, M., Mendez, L., Shaknovich, R., Cole, P.A., et al. (2010b). BCL6

repression of EP300 in human diffuse large B cell lymphoma cells provides a basis for rational combinatorial therapy. J. Clin. Invest. *120*, 4569–4582.

Compagno, M., Lim, W.K., Grunn, A., Nandula, S.V., Brahmachary, M., Shen, Q., Bertoni, F., Ponzoni, M., Scandurra, M., Califano, A., et al. (2009). Mutations of multiple genes cause deregulation of NF-κB in diffuse large B-cell lymphoma. Nature *459*, 717–721.

Coornaert, B., Baens, M., Heyninck, K., Bekaert, T., Haegman, M., Staal, J., Sun, L., Chen, Z.J., Marynen, P., and Beyaert, R. (2008). T cell antigen receptor stimulation induces MALT1 paracaspase-mediated cleavage of the NF-κB inhibitor A20. Nat. Immunol. *9*, 263–271.

Davis, R.E., Ngo, V.N., Lenz, G., Tolar, P., Young, R.M., Romesser, P.B., Kohlhammer, H., Lamy, L., Zhao, H., Yang, Y., et al. (2010). Chronic active B-cell-receptor signalling in diffuse large B-cell lymphoma. Nature *463*, 88–92.

Dierlamm, J., Baens, M., Wlodarska, I., Stefanova-Ouzounova, M., Hernandez, J.M., Hossfeld, D.K., De Wolf-Peeters, C., Hagemeijer, A., Van den Berghe, H., and Marynen, P. (1999). The apoptosis inhibitor gene API2 and a novel 18q gene, MLT, are recurrently rearranged in the t(11;18)(q21;q21) associated with mucosa-associated lymphoid tissue lymphomas. Blood *93*, 3601–3609.

Dierlamm, J., Murga Penas, E.M., Bentink, S., Wessendorf, S., Berger, H., Hummel, M., Klapper, W., Lenze, D., Rosenwald, A., Haralambieva, E., et al.; Deutsche Krebshilfe Network Project "Molecular Mechanisms in Malignant Lymphomas". (2008). Gain of chromosome region 18q21 including the MALT1 gene is associated with the activated B-cell-like gene expression subtype and increased BCL2 gene dosage and protein expression in diffuse large B-cell lymphoma. Haematologica *93*, 688–696.

Farinha, P., and Gascoyne, R.D. (2005). Molecular pathogenesis of mucosa-associated lymphoid tissue lymphoma. J. Clin. Oncol. *23*, 6370–6378.

Ferch, U., zum Büschenfelde, C.M., Gewies, A., Wegener, E., Rauser, S., Peschel, C., Krappmann, D., and Ruland, J. (2007). MALT1 directs B cell receptor-induced canonical nuclear factor-κB signaling selectively to the c-Rel subunit. Nat. Immunol. *8*, 984–991.

Ferch, U., Kloo, B., Gewies, A., Pfänder, V., Düwel, M., Peschel, C., Krappmann, D., and Ruland, J. (2009). Inhibition of MALT1 protease activity is selectively toxic for activated B cell-like diffuse large B cell lymphoma cells. J. Exp. Med. *206*, 2313–2320.

Genin, E., Reboud-Ravaux, M., and Vidal, J. (2010). Proteasome inhibitors: recent advances and new perspectives in medicinal chemistry. Curr. Top. Med. Chem. *10*, 232–256.

Gross, O., Grupp, C., Steinberg, C., Zimmermann, S., Strasser, D., Hannesschläger, N., Reindl, W., Jonsson, H., Huo, H., Littman, D.R., et al. (2008). Multiple ITAM-coupled NK-cell receptors engage the Bcl10/Malt1 complex via Carma1 for NF-κB and MAPK activation to selectively control cytokine production. Blood *112*, 2421–2428.

Hachmann, J., Snipas, S.J., van Raam, B.J., Cancino, E.M., Houlihan, E.J., Poreba, M., Kasperkiewicz, P., Drag, M., and Salvesen, G.S. (2012). Mechanism and specificity of the human paracaspase MALT1. Biochem. J. *443*, 287–295.

Hailfinger, S., Lenz, G., Ngo, V., Posvitz-Fejfar, A., Rebeaud, F., Guzzardi, M., Penas, E.M., Dierlamm, J., Chan, W.C., Staudt, L.M., and Thome, M. (2009). Essential role of MALT1 protease activity in activated B cell-like diffuse large B-cell lymphoma. Proc. Natl. Acad. Sci. USA *106*, 19946–19951.

Hailfinger, S., Nogai, H., Pelzer, C., Jaworski, M., Cabalzar, K., Charton, J.E., Guzzardi, M., Décaillet, C., Grau, M., Dörken, B., et al. (2011). Malt1-dependent RelB cleavage promotes canonical NF-κB activation in lymphocytes and lymphoma cell lines. Proc. Natl. Acad. Sci. USA *108*, 14596–14601.

Hans, C.P., Weisenburger, D.D., Greiner, T.C., Gascoyne, R.D., Delabie, J., Ott, G., Müller-Hermelink, H.K., Campo, E., Braziel, R.M., Jaffe, E.S., et al. (2004). Confirmation of the molecular classification of diffuse large B-cell lymphoma by immunohistochemistry using a tissue microarray. Blood *103*, 275–282.

Honigberg, L.A., Smith, A.M., Sirisawad, M., Verner, E., Loury, D., Chang, B., Li, S., Pan, Z., Thamm, D.H., Miller, R.A., and Buggy, J.J. (2010). The Bruton tyrosine kinase inhibitor PCI-32765 blocks B-cell activation and is efficacious in models of autoimmune disease and B-cell malignancy. Proc. Natl. Acad. Sci. USA *107*, 13075–13080.

Honma, K., Tsuzuki, S., Nakagawa, M., Tagawa, H., Nakamura, S., Morishima, Y., and Seto, M. (2009). TNFAIP3/A20 functions as a novel tumor suppressor gene in several subtypes of non-Hodgkin lymphomas. Blood *114*, 2467–2475.

Klibanov, O.M., Williams, S.H., Smith, L.S., Olin, J.L., and Vickery, S.B. (2011). Telaprevir: a novel NS3/4 protease inhibitor for the treatment of hepatitis C. Pharmacotherapy *31*, 951–974.

Lenz, G., and Staudt, L.M. (2010). Aggressive lymphomas. N. Engl. J. Med. *362*, 1417–1429.

Lenz, G., Davis, R.E., Ngo, V.N., Lam, L., George, T.C., Wright, G.W., Dave, S.S., Zhao, H., Xu, W., Rosenwald, A., et al. (2008a). Oncogenic CARD11 mutations in human diffuse large B cell lymphoma. Science *319*, 1676–1679.

Lenz, G., Wright, G.W., Emre, N.C., Kohlhammer, H., Dave, S.S., Davis, R.E., Carty, S., Lam, L.T., Shaffer, A.L., Xiao, W., et al. (2008b). Molecular subtypes of diffuse large B-cell lymphoma arise by distinct genetic pathways. Proc. Natl. Acad. Sci. USA *105*, 13520–13525.

Lim, K.H., Yang, Y., and Staudt, L.M. (2012). Pathogenetic importance and therapeutic implications of NF-κB in lymphoid malignancies. Immunol. Rev. *246*, 359–378.

Lucas, P.C., Yonezumi, M., Inohara, N., McAllister-Lucas, L.M., Abazeed, M.E., Chen, F.F., Yamaoka, S., Seto, M., and Nunez, G. (2001). Bcl10 and MALT1, independent targets of chromosomal translocation in MALT lymphoma, cooperate in a novel NF-κB signaling pathway. J. Biol. Chem. *276*, 19012–19019.

Manicassamy, S. (2009). Sotrastaurin, a protein kinase C inhibitor for the prevention of transplant rejection and treatment of psoriasis. Curr. Opin. Investig. Drugs *10*, 1225–1235.

Matz, M., Naik, M., Mashreghi, M.F., Glander, P., Neumayer, H.H., and Budde, K. (2011). Evaluation of the novel protein kinase C inhibitor sotrastaurin as immunosuppressive therapy after renal transplantation. Expert Opin. Drug Metab. Toxicol. *7*, 103–113.

Misale, S., Yaeger, R., Hobor, S., Scala, E., Janakiraman, M., Liska, D., Valtorta, E., Schiavo, R., Buscarino, M., Siravegna, G., et al. (2012). Emergence of KRAS mutations and acquired resistance to anti-EGFR therapy in colorectal cancer. Nature *486*, 532–536.

Morris, G.M., Huey, R., Lindstrom, W., Sanner, M.F., Belew, R.K., Goodsell, D.S., and Olson, A.J. (2009). AutoDock4 and AutoDockTools4: automated docking with selective receptor flexibility. J. Comput. Chem. *30*, 2785–2791.

Naylor, T.L., Tang, H., Ratsch, B.A., Enns, A., Loo, A., Chen, L., Lenz, P., Waters, N.J., Schuler, W., Dörken, B., et al. (2011). Protein kinase C inhibitor sotrastaurin selectively inhibits the growth of CD79 mutant diffuse large B-cell lymphomas. Cancer Res. *71*, 2643–2653.

Ngo, V.N., Davis, R.E., Lamy, L., Yu, X., Zhao, H., Lenz, G., Lam, L.T., Dave, S., Yang, L., Powell, J., and Staudt, L.M. (2006). A loss-of-function RNA interference screen for molecular targets in cancer. Nature *441*, 106–110.

Ngo, V.N., Young, R.M., Schmitz, R., Jhavar, S., Xiao, W., Lim, K.H., Kohlhammer, H., Xu, W., Yang, Y., Zhao, H., et al. (2011). Oncogenically active MYD88 mutations in human lymphoma. Nature *470*, 115–119.

Polo, J.M., Dell'Oso, T., Ranuncolo, S.M., Cerchietti, L., Beck, D., Da Silva, G.F., Prive, G.G., Licht, J.D., and Melnick, A. (2004). Specific peptide interference reveals BCL6 transcriptional and oncogenic mechanisms in B-cell lymphoma cells. Nat. Med. *10*, 1329–1335.

Pop, C., Timmer, J., Sperandio, S., and Salvesen, G.S. (2006). The apoptosome activates caspase-9 by dimerization. Mol. Cell *22*, 269–275.

Powers, J.C., Asgian, J.L., Ekici, O.D., and James, K.E. (2002). Irreversible inhibitors of serine, cysteine, and threonine proteases. Chem. Rev. *102*, 4639–4750.

Rebeaud, F., Hailfinger, S., Posevitz-Fejfar, A., Tapernoux, M., Moser, R., Rueda, D., Gaide, O., Guzzardi, M., Iancu, E.M., Rufer, N., et al. (2008). The proteolytic activity of the paracaspase MALT1 is key in T cell activation. Nat. Immunol. *9*, 272–281.

Rosenwald, A., Wright, G., Chan, W.C., Connors, J.M., Campo, E., Fisher, R.I., Gascoyne, R.D., Muller-Hermelink, H.K., Smeland, E.B., Giltnane, J.M., et al.; Lymphoma/Leukemia Molecular Profiling Project. (2002). The use of molecular

profiling to predict survival after chemotherapy for diffuse large-B-cell lymphoma. N. Engl. J. Med. *346*, 1937–1947.

Rosenwald, A., Wright, G., Leroy, K., Yu, X., Gaulard, P., Gascoyne, R.D., Chan, W.C., Zhao, T., Haioun, C., Greiner, T.C., et al. (2003). Molecular diagnosis of primary mediastinal B cell lymphoma identifies a clinically favorable subgroup of diffuse large B cell lymphoma related to Hodgkin lymphoma. J. Exp. Med. *198*, 851–862.

Ruefli-Brasse, A.A., French, D.M., and Dixit, V.M. (2003). Regulation of NF-κB-dependent lymphocyte activation and development by paracaspase. Science *302*, 1581–1584.

Ruland, J., Duncan, G.S., Wakeham, A., and Mak, T.W. (2003). Differential requirement for Malt1 in T and B cell antigen receptor signaling. Immunity *19*, 749–758.

Sanchez-Izquierdo, D., Buchonnet, G., Siebert, R., Gascoyne, R.D., Climent, J., Karran, L., Marin, M., Blesa, D., Horsman, D., Rosenwald, A., et al. (2003). MALT1 is deregulated by both chromosomal translocation and amplification in B-cell non-Hodgkin lymphoma. Blood *101*, 4539–4546.

Siegel, R., Naishadham, D., and Jemal, A. (2012). Cancer statistics, 2012. CA Cancer J. Clin. *62*, 10–29.

Staal, J., Driege, Y., Bekaert, T., Demeyer, A., Muyllaert, D., Van Damme, P., Gevaert, K., and Beyaert, R. (2011). T-cell receptor-induced JNK activation requires proteolytic inactivation of CYLD by MALT1. EMBO J. *30*, 1742–1752.

Streubel, B., Lamprecht, A., Dierlamm, J., Cerroni, L., Stolte, M., Ott, G., Raderer, M., and Chott, A. (2003). T(14;18)(q32;q21) involving IGH and MALT1 is a frequent chromosomal aberration in MALT lymphoma. Blood *101*, 2335–2339.

Swerdlow, S.H., Campo, E., Harris, N.L., Jaffe, E.S., Pileri, S.A., Stein, H., Thiele, J., and Vardiman, J.W. (2008). World Health Organization Classification of Tumours of Haematopoietic and Lymphoid Tissues (Lyon: IARC Press).

Vicente-Dueñas, C., Fontán, L., Gonzalez-Herrero, I., Romero-Camarero, I., Segura, V., Aznar, M.A., Alonso-Escudero, E., Campos-Sanchez, E., Ruiz-Roca, L., Barajas-Diego, M., et al. (2012). Expression of MALT1 oncogene in hematopoietic stem/progenitor cells recapitulates the pathogenesis of human lymphoma in mice. Proc. Natl. Acad. Sci. USA *109*, 10534–10539.

Walker, N.P., Talanian, R.V., Brady, K.D., Dang, L.C., Bump, N.J., Ferenz, C.R., Franklin, S., Ghayur, T., Hackett, M.C., Hammill, L.D., et al. (1994). Crystal structure of the cysteine protease interleukin-1β-converting enzyme: a (p20/p10)2 homodimer. Cell *78*, 343–352.

Wiesmann, C., Leder, L., Blank, J., Bernardi, A., Melkko, S., Decock, A., D'Arcy, A., Villard, F., Erbel, P., Hughes, N., et al. (2012). Structural determinants of MALT1 protease activity. J. Mol. Biol. *419*, 4–21.

Wright, G., Tan, B., Rosenwald, A., Hurt, E.H., Wiestner, A., and Staudt, L.M. (2003). A gene expression-based method to diagnose clinically distinct subgroups of diffuse large B cell lymphoma. Proc. Natl. Acad. Sci. USA *100*, 9991–9996.

Yin, Q., Park, H.H., Chung, J.Y., Lin, S.C., Lo, Y.C., da Graca, L.S., Jiang, X., and Wu, H. (2006). Caspase-9 holoenzyme is a specific and optimal procaspase-3 processing machine. Mol. Cell *22*, 259–268.

Yu, J.W., Jeffrey, P.D., Ha, J.Y., Yang, X., and Shi, Y. (2011). Crystal structure of the mucosa-associated lymphoid tissue lymphoma translocation 1 (MALT1) paracaspase region. Proc. Natl. Acad. Sci. USA *108*, 21004–21009.

Zhang, J.H., Chung, T.D., and Oldenburg, K.R. (1999). A simple statistical parameter for use in evaluation and validation of high throughput screening assays. J. Biomol. Screen. *4*, 67–73.